Supplementary Information

Position-sensitive spectral splitting with a plasmonic nanowire on silicon chip

Qing Hu[1,2], Di-Hu Xu[1], Yu Zhou[1], Ru-Wen Peng[1,*], Ren-Hao Fan[1], Nicholas X. Fang[2], Qian-Jin Wang[1], Xian-Rong Huang[3], and Mu Wang[1,*]

1) National Laboratory of Solid State Microstructures and Department of Physics, Nanjing University, Nanjing 210093, China

2) Department of Mechanical Engineering, Massachusetts Institute of Technology, Cambridge, Massachusetts 02139, USA

3) Advanced Photon Source, Argonne National Laboratory, Argonne, Illinois 60439, USA

Outline

Supplementary Figures

Supplementary Calculation and Analysis

1. **Surface plasmon modes on Ag nanowire atop Si wafer**
2. **Plasmonic band gaps of corrugated Ag nanowire atop Si wafer**

Supplementary Experiments and Discussions

1. **Experimental setup and measurement**
2. **Additional experimental demonstrations**
3. **Side-band suppression and outcoupling efficiency**
4. **Discrepancy between experiments and simulations**
5. **Propagation performances of the plasmonic PSS and SOI nanowire at visible regime**

Supplementary Figures

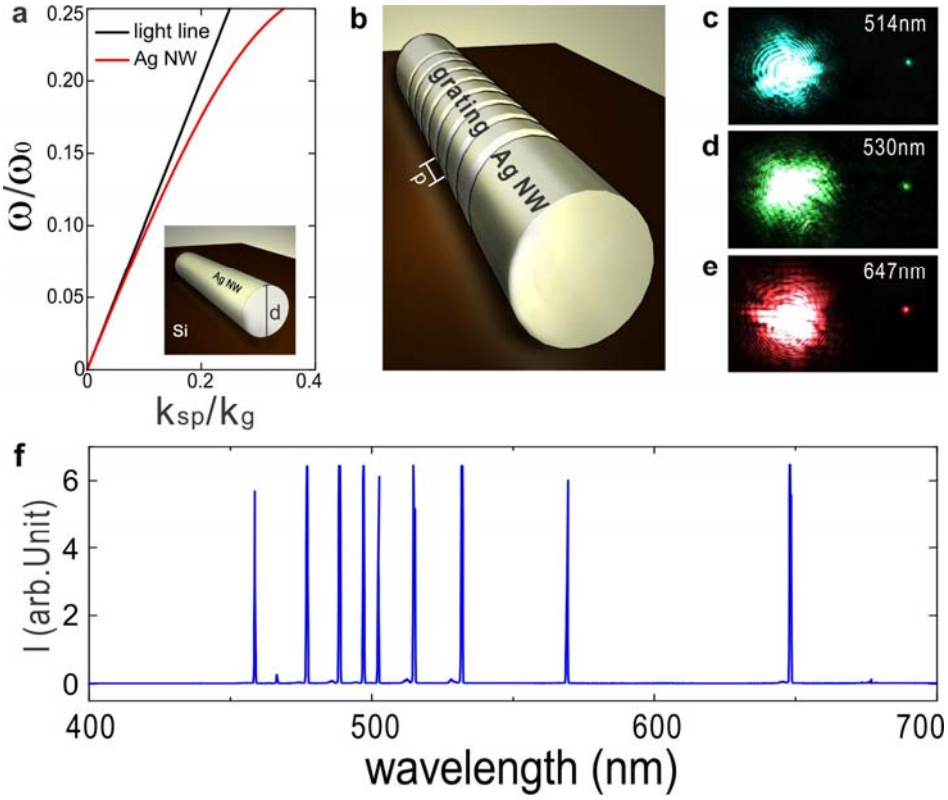

Supplementary Figure S1 | SP propagation on Ag nanowire atop Si wafer. a. Dispersion relation of a smooth non-corrugated silver nanowire on a Si substrate showing a wide continuous frequency range. Inset: schematic of silver nanowire with radius (d=170nm) on Si wafer. Microscopic images taken by CCD for illuminated laser source with wavelength as **c.** 514nm; **d.** 530nm; **e.** 647nm, respectively. **f.** Measured output spectra of a silver nanowire with length around 8μm under multiple lasers illumination with the wavelengths as 488nm, 514nm, 520nm, 530nm, 568nm, 647nm.

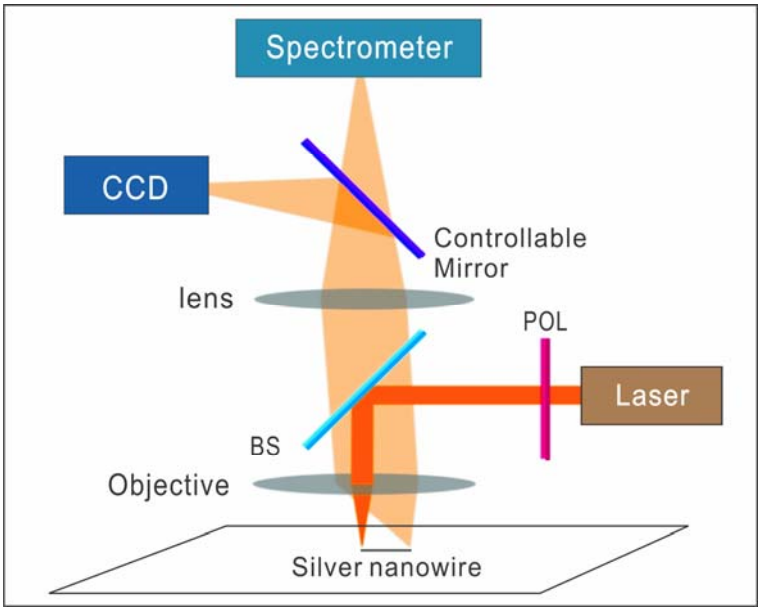

Supplementary Figure S2 | Experimental setups. POL: polarizer; BS: beam splitter. The input laser beam (with main wavelengths as 647 nm, 568 nm, 530 nm, 520 nm, 514 nm, 488 nm from Spectra-Physics Lasers, 2018-RM) is focused by an objective (100x) to the end or the middle of the nanowire. The emitted light is analyzed by a spectrometer (Princeton Instruments，SP-2500). The emission from the microstructured nanowire is imaged by a CCD. The spectrum measurement and the emission imaging are switchable by a controllable mirror.

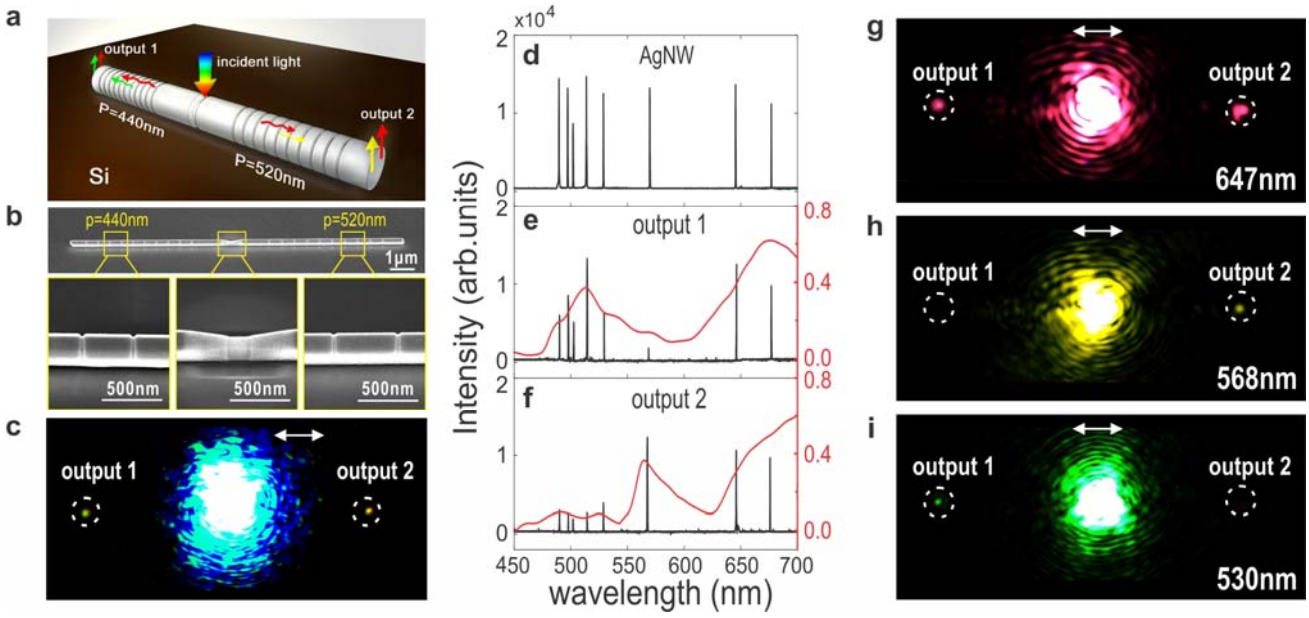

Supplementary Figure S3 | The additional experiment for parallel plasmonic PSS based on a 260nm-diameter Ag nanowire consisting of two corrugated gratings with periodicity as 440nm and 520nm, respectively. a. Schematic of the structured silver nanowire with two corrugated gratings (with periods P = 440 nm and P = 520 nm) separated by a single groove in the middle that converts the incident beam into SPs propagating towards the two ends of the nanowire. **b.** SEM images of the nanowire and the enlarged structure details. **c.** The corresponding emission images for a multiple-wavelength laser beam. **d.** Scattered light spectra measured from the end of a smooth nanowire with no corrugations. **e, f.** Experimental (black lines) and calculated (red lines) spectra taken from "output1" and "output2" of the corrugated nanowire, respectively. **g-i.** Emission images of "output1", the middle groove, and "output2" for incident wavelengths of 647nm, 568nm and 530nm, respectively.

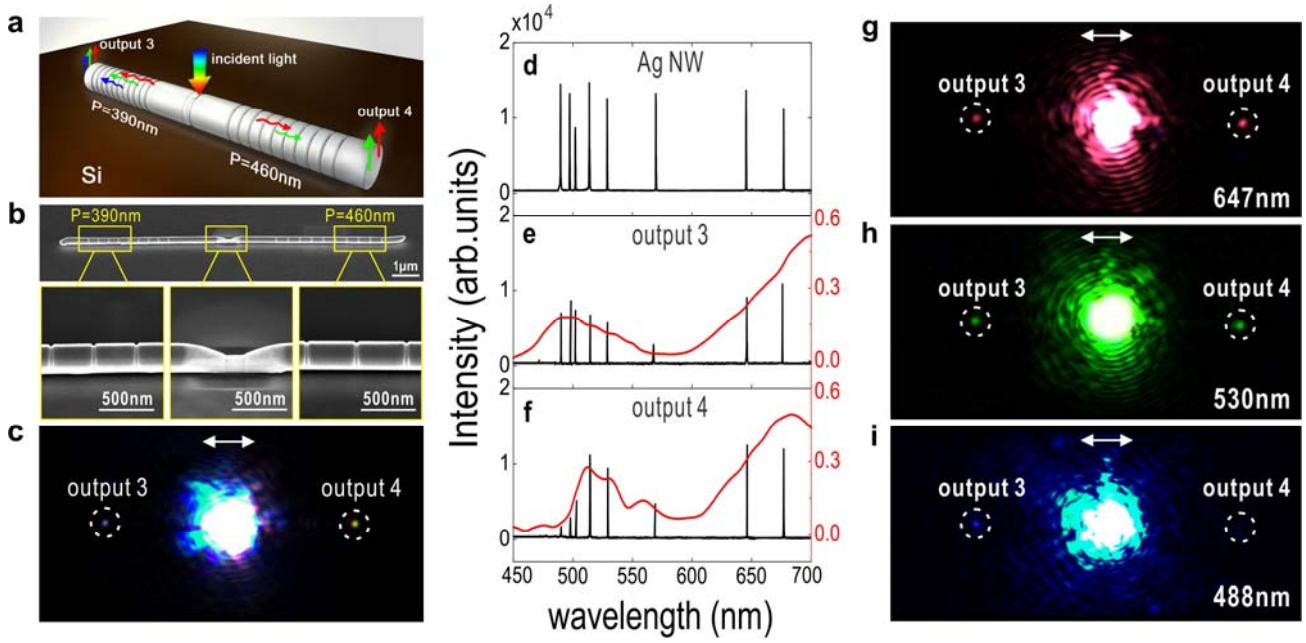

Supplementary Figure S4 | The additional experiment for parallel plasmonic PSS based on a 260nm-diameter Ag nanowire consisting of two corrugated gratings with periodicity as 390nm and 460nm, respectively. a. Schematic of the structured silver nanowire with two corrugated gratings (with periods P = 390 nm and P = 460 nm) separated by a single groove in the middle that converts the incident beam into SPs propagating towards the two ends of the nanowire. **b.** SEM images of the nanowire and the enlarged structure details. **c.** The corresponding emission images for a multiple-wavelength laser beam. **d.** Scattered light spectra measured from the end of a smooth nanowire with no corrugations. **e, f.** Experimental (black lines) and calculated (red lines) spectra taken from "output3" and "output4" of the corrugated nanowire, respectively. **g-i.** Emission images of "output3", the middle groove, and "output4" for incident wavelengths of 647nm, 530nm and 488nm, respectively. The white double-arrow segment in **c, g-i** indicates the polarization direction of the input beam.

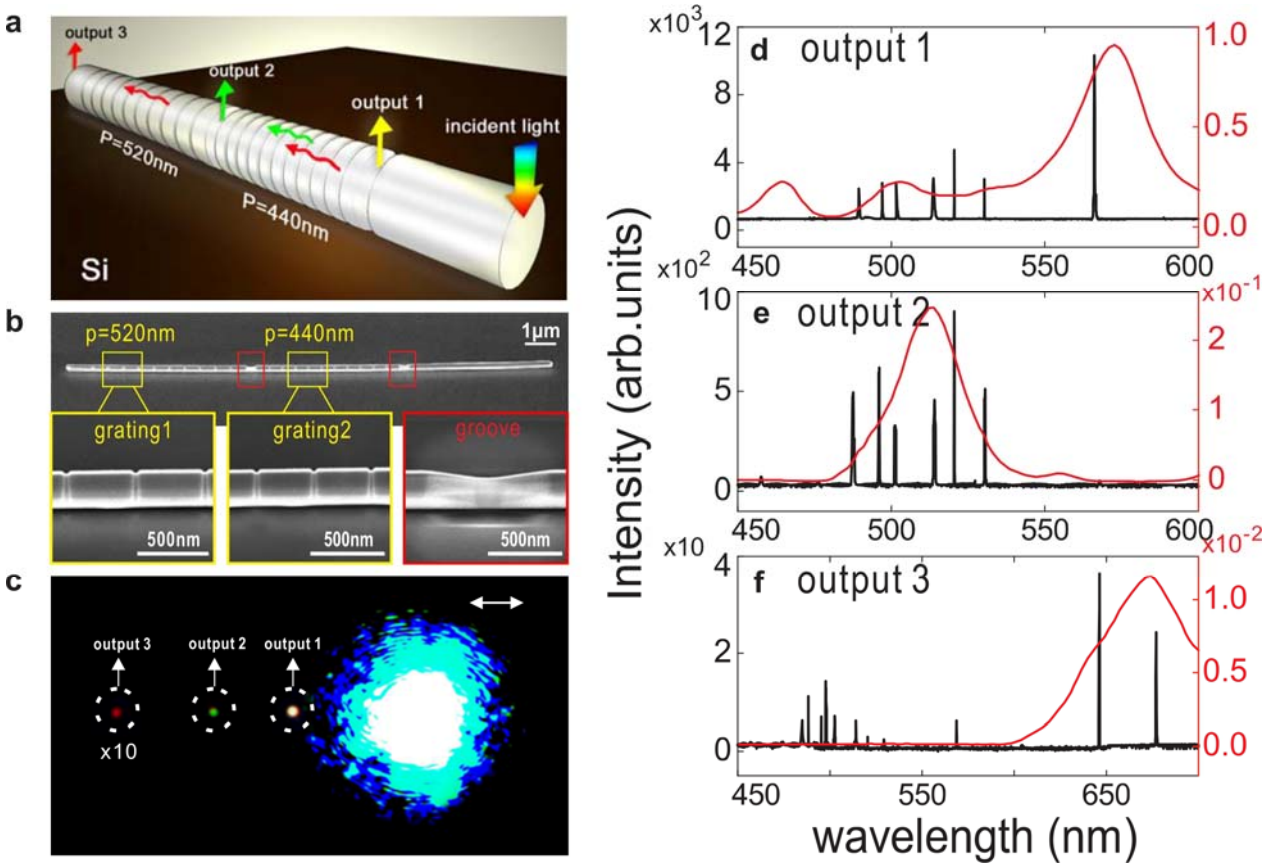

Supplementary Figure S5 | The additional experiment for cascaded plasmonic PSS based on a 260nm-diameter Ag nanowire consisting of two corrugated gratings with periodicity as 440nm and 520nm, respectively). a. Schematic illustration of a silver nanowire with cascading corrugation with period P=440nm (termed as Grating 2) and P=520nm (termed as Grating 1), respectively. Two grooves are marked as "Output 1" and "Output 2", respectively. **b.** SEM images of the configuration of the structures: corrugations with P=520nm (left), corrugations with P=440nm (middle), and one groove (right). **c.** Emission micrograph of the structured nanowire illuminated by a multiple-wavelength laser beam from the input end (right most). The bright spots marked by the dash white circles indicate the light scattered from grooves as "output1", "output2" and "output3". The white double-arrow segment indicates the polarization direction of the input beam. **d-f.** Experimental (black lines) and calculated (red lines) scattered light spectra taken from sites "output1", "output2" and "output3", respectively.

Supplementary Calculations and Analysis

1. Surface plasmon modes on Ag nanowire atop Si wafer

The dispersion relation of the SP mode on smooth Ag nanowire on Si wafer can be calculated by using Finite Element Method (Comsol 3.5a). As shown in Fig. S1a, the dispersion is continuous in a wide frequency region, which means the Ag nanowire supports a broadband SP mode. In the experiments, we deposit the chemically synthesized Ag nanowires [S1] (with radius around 85nm) on the surface of Si wafer. When focusing laser beams at one distal facet, the surface plasmons can be launched to propagate along the nanowire axis, then couple to far field light at wire discontinuities [S2]. The scattering images at different propagation wavelengths (514nm, 530nm, 647nm) are detected with a charge-couple-device camera (CCD) camera (Fig. S1c-e), respectively. The spectra are measured by a spectrometer under illuminations of multiple lasers with main wavelengths as 488nm, 514nm, 520nm, 530nm, 568nm, 647nm (Fig. S1f). These figures demonstrate that the Ag nanowires on Si wafer are able to support SP modes at a wide frequency range.

To evaluate the propagating properties of the SPs, the effective mode index (n_{eff}) and propagating length (L) are calculated by using finite element method. Here the effective index and propagating length are defined as $n_{eff} = \beta / k_0$ and $L = 1/2\,\mathrm{Im}\{\beta\}$, respectively, where β is the propagation constant of the SP mode and k_0 is the wave vector in vacuum, respectively. As shown in Fig.S6a, with the refractive index of the substrate increasing, n_{eff} increases, while L decreases. It indicates that the higher-refractive-index substrate results in higher loss, and the hybrid gap mode has higher loss than the axis-symmetric mode. The mode profiles in the three situations are shown in Fig. S6b-d. It can be seen that due to the high-refractive index and optical absorption of Si, most of the electric energy is confined in the gap between Ag nanowire and Si substrate (Fig. S6d). When decreasing refractive index of substrate, more electric energy lies in the substrate (Fig.S6c). Further decreasing the refractive index until there is no difference of the refractive index between surrounding media and substrate material leads to an axis-symmetric SP mode (Fig.S6 b). These results indicate that the nanowire sustains a hybrid gap mode of SPs at the presence of substrate. The profile of the hybrid mode shows great dependence on the refractive index of substrates. The similar phenomenon has been reported in Ref. S3-S5.

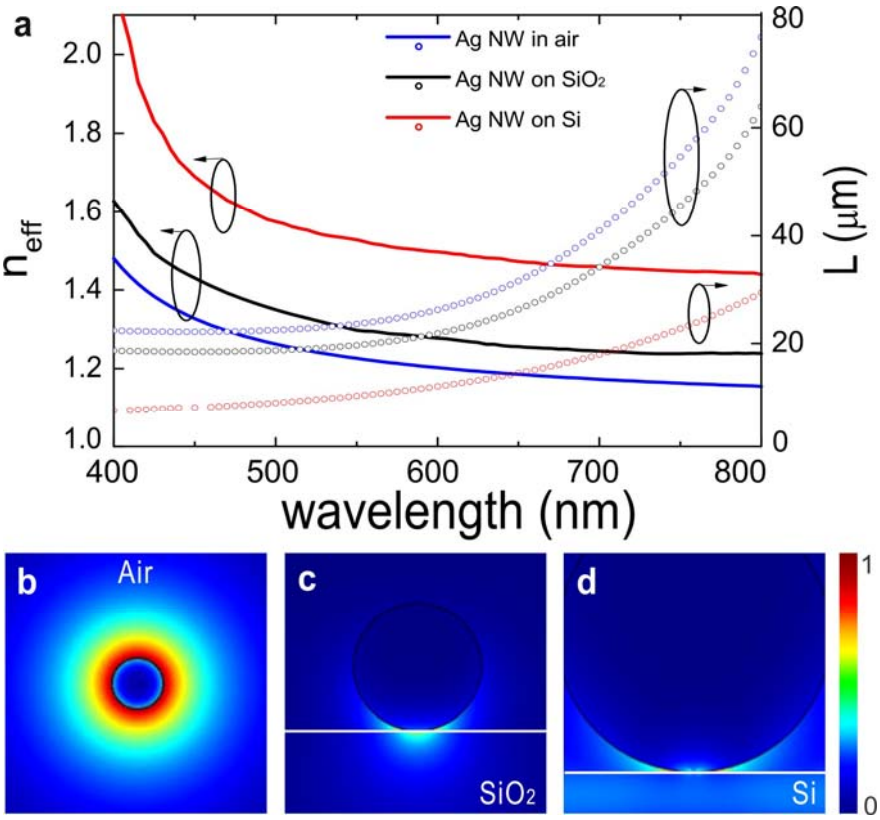

Supplementary Figure S6 | Propagation behavior of SP mode on Ag nanowire. a. Effective Mode index and propagation length of SP modes sustained by Ag nanowire with a diameter as 170nm in air, on SiO_2 substrate, and on Si substrate, respectively. Mode profiles of the SP modes (647nm) sustained by Ag nanowire **b** in air. **c** on SiO_2 substrate. **d** on Si substrate (enlarged shows the electric energy in the gap), respectively.

In addition to the effective mode index and propagation loss, the effective mode area A_m has also been investigated. The effective mode area A_m is defined as the ratio of mode energy per unit length along the direction of propagation and its peak energy density, such that [S6]

$$A_m = \frac{W_m}{\max\{W(r)\}} = \frac{1}{\max\{W(r)\}} \int_{-\infty}^{\infty} W(r)\, d^2 r \qquad (1)$$

where W_m and $W(r)$ are the electromagnetic energy and energy density (per unit length along the direction of propagation), respectively:

$$W(r) = \frac{1}{2}\left(\frac{d(\varepsilon(r)\omega)}{d\omega} |E(r)|^2 + \mu_0 |H(r)|^2 \right) \qquad (2)$$

We calculate the normalized ode area A (defined as A_m / A_0, where A_0 is the diffraction-limited area in free space with the value as $\lambda^2/4$) of Ag nanowire with different sizes (170nm and 260nm radius, respectively) at visible region. Here the Ag nanowire is coated with 5nm SiO_2, positioned on top of Si substrate, which is the same as the experimental situation. As shown in Fig. S7a, the mode area of 260nm Ag nanowire is lower than 0.2. When decreasing the diameter of Ag nanowire to 170nm, the mode area is smaller. At some wavelength points, e.g.568nm, it can reach 0.02. Therefore the confinement could be enhanced by scaling down the size of nanowire. From the mode profiles (Fig. S7b,c), we can see that the electric energy is both confined around the surface of SiO_2 coated Ag nanowire and in the gap between the nanowire and the substrate. Thus the modes are hybrid SP modes.

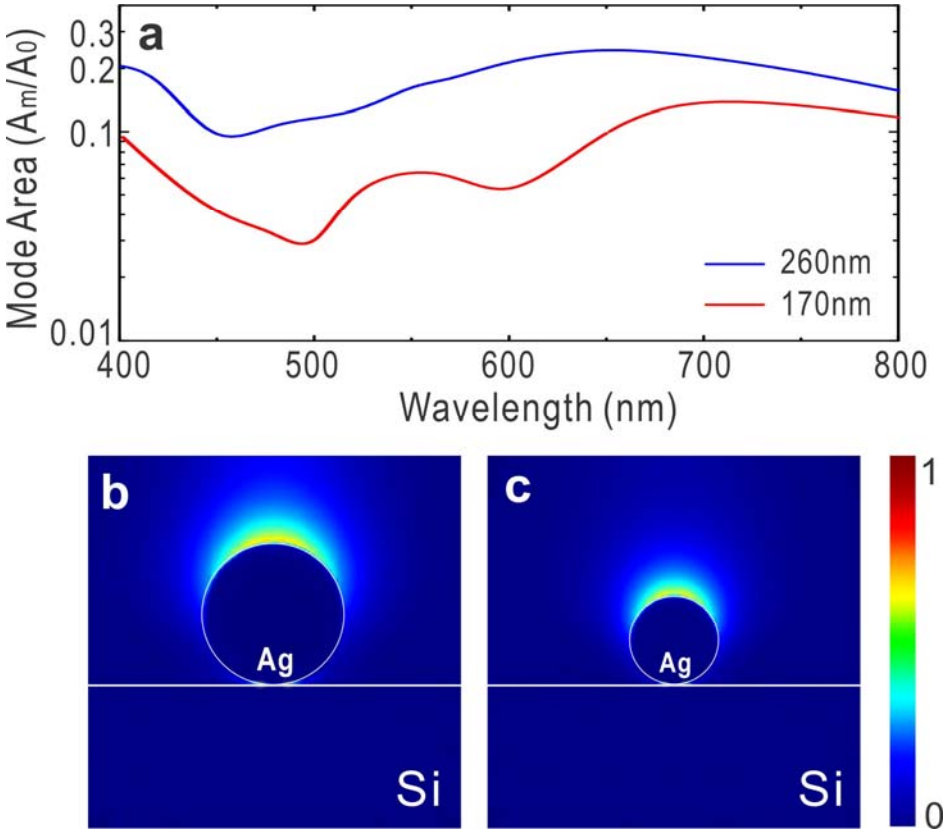

Supplementary Figure S7 | Effective mode area and mode profile of SPs on Ag nanowire with 5nm SiO_2 coating layer. a Effective mode areas of SPs on Ag nanowire with different diameters (blue line: 260nm, red line: 170nm) atop Si substrate. Here the values of mode areas are plotted on a logarithmic scale. **b,c** Mode profiles at the wavelength as 647nm for 260nm-diameter and 170nm-diameter nanowires, respectively. The data is calculated by using FDTD method (Lumerical 8.0.1).

2. Plasmonic band gaps of corrugated Ag nanowire atop Si wafer

For a suspended metallic cylindrical waveguide whose diameter is reduced to several hundreds of nanometer, only the fundamental (azimuthally symmetric) transverse magnetic SP mode exists [S7]. According to the solutions of Maxwell's equations in cylindrical coordinate and the boundary conditions of SP wave, the dispersion of a metallic nanowire (ε_1 , R_1) coated a dielectric layer (ε_2 , R_2) embedded in a medium (ε_3) can be derived as

$$\varepsilon_1 k_1 I_1(k_1 R_1)\left[\varepsilon_3 k_2 K_1(k_3 R_2) M_{00} + \varepsilon_2 k_3 K_0(k_3 R_2) M_{10}\right] = -\varepsilon_2 k_1 I_0(k_1 R_1)\left[\varepsilon_3 k_2 K_1(k_3 R_2) M_{01} + \varepsilon_2 k_3 K_0(k_3 R_2) M_{11}\right] \tag{3}$$

where

$$M_{ab} = I_a(k_2 R_2) K_b(k_2 R_1) - (-1)^{a+b} I_b(k_2 R_1) K_a(k_2 R_2) \tag{4}$$

$k_j = (\beta^2 - \varepsilon_j k^2)^{1/2}$, I_a and K_a are the modified Bessel functions of the first and second kinds, respectively. The calculated dispersions of the SP mode are shown in Fig.S8a. It can be seen that SP mode of Ag nanowire with larger radius approaches to the mode on an Ag-air surface, which indicates a similar behavior of the SP mode between the metallic nanowire and planar cases. Therefore the metallic nanowire can be approximately treated as a planar metallic surface.

For a metallic nanowire atop a silicon wafer, by optimizing the permittivity of dielectric (ε=2.7 in our case), the dispersion of a planar Ag-dielectric surface can be fitted to that of a 5nm-SiO_2 coating Ag nanowire (Fig. S8b). Thus the coated Ag nanowire is reasonable to be treated as a planar Ag-dielectric surface. Therefore it is reasonable to apply the planar Ag/dielectric model to generate the calculations results in SiO_2-coating Ag nanowire structure. Under the approximation situation, by using the rigorous coupled-wave analysis (RCWA) method [S8], angular-dependent reflection spectra can be generated to describe the plasmonic band gaps. In the reflection spectra (as shown in Fig 1b), the minimum reflectivity corresponds to the photons that have been absorbed through the excitation of SPs. Therefore the green-blue arcs in the figures denote the dispersions of the SP modes on the textured Ag nanowire. Due to the periodically corrugations, photonic gaps appear at the Brillouin zone edges, where the SPs are back-reflected so strongly that they cannot propagate any more. With increasing the periodicity of the corrugations, the central frequencies of the plasmonic gaps have red shifts. Besides, one more band gap appears at high frequency region.

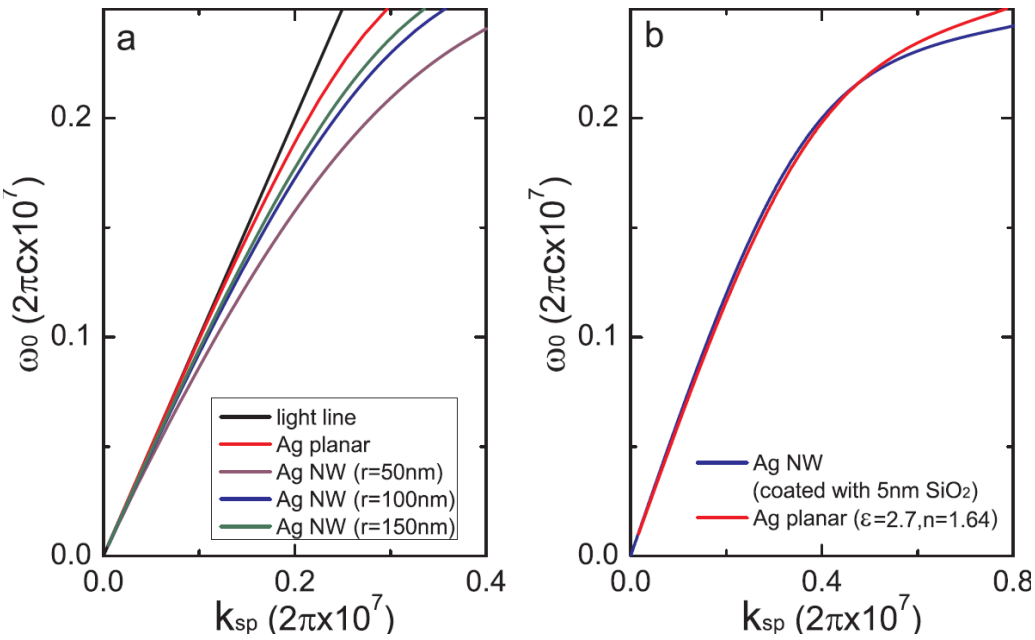

Supplementary Figure S8 | Dispersion relations of SP modes on Ag nanowires and Ag planar. a Dispersion relations of SP modes on Ag nanowires with different radiuses. **b** Dispersion relation of a planar Ag-dielectric film (the permittivity of dielectric is set as 2.7) agrees well with that of a 5nm-SiO_2-coated Ag nanowire.

Supplementary Experiments and Discussions

1. Experimental setup and measurement

We measure the spectra by using a confocal micro spectrometer system. As schematically shown in Fig. S2, the input laser beam (Spectra-Physics Lasers, 2018-RM with main wavelengths as 647nm, 568nm, 530nm, 520nm, 514nm, 488nm) is focused on the input positions (the distal ends or the grooves in the middle) by an objective (100x). The emitted spectra are measured by a spectrometer (Princeton Instruments，SP-2500). The scattered image is detected by a CCD. The spectrum measurement and the emission imaging are switchable by a controllable mirror. In the measurement, we fix the laser power, tilting the beam splitter (shown in Fig. S2) to focus the incident laser on the input terminals. Slightly tune the objective focusing to find largest scattered intensities, then record the spectra.

2. Additional experimental demonstrations

To confirm the functions of the plasmonic PSS, we fabricate the similar structures on 130nm-radius silver nanowires. We firstly fabricated the parallel PSS, in which two corrugations with periodicities P=440nm and P=520nm are separated by a single groove (Fig. S3a,b). When focusing the laser beam on the groove, the SPs are excited to propagate towards the two ends of the nanowire. Due to the manipulation of plasmonic band gaps of the two gratings, the SPs on the silver nanowire are selected to propagate, thus the output colors at the two ends are different (Fig. S3g-i). The optical spectra of the scattered light are measured at the two ends (Fig. S3e,f). Compared with the spectra of a smooth silver nanowire (Fig. S3d), the intensity for λ=568nm drops at “output1” in Fig S3e, while the intensities for λ=514, 520, 530nm attenuate obviously at “output2” in Fig. S3f. These measured data are in good agreement with the calculated normalized transmission (red lines in Fig. S3e,f). We further fabricate another parallel PSS with different grating periodicities as 390nm and 460nm. As shown in Fig. S4, the propagation of SPs are tuned by the plasmonic band gap, and different frequencies are selected to output at the two ends. Then we fabricate the cascaded PSS. As shown in Fig. S5a-b, the structure consists of two gratings with periods as P=440nm (grating 2) and P=520nm (grating 1), respectively, and two grooves termed as “output 1” and “output 2”, respectively. Because the plasmonic band gaps of the gratings forbid some frequencies and let the others go through, different colors of the released light from the grooves. From the scattering image detected by CCD (Fig. S5c), we observe a yellow bright spot at “output1” and a green bright spot at “output2”. Figure S5d-f show the

optical spectra measured by the spectrometer (black lines), together with the calculated ones (red curves). These measured and calculated spectra are in agreement with each other. With these data, we confirm that the cascaded PSS can be realized based on the structured silver nanowire. It should be noted that because the difference of the effective mode index between the Ag nanowires with radius as 85nm and 130nm is small, the gratings on the two types of Ag nanowires have nearly the same periods (520nm & 470nm for 85nm-radius nanowire and 520nm & 440nm for 130nm-radius nanowire).

3. Side-band suppression and outcoupling efficiency

We perform FDTD simulation (Lumerical 8.0.1) to get the side-band suppression data. In the simulation, the scattering energy are collected from the output positions of two kinds of nanowires without grating coupler ($I_0(\lambda)$) and with grating coupler ($I(\lambda)$). Then the side-band suppression is calculated as

$$S_{dB}(\lambda) = -10\log_{10}[I(\lambda)/I_0(\lambda)] \quad (1)$$

This parameter evaluates the ability of the grating to forbid the SPs in the band gaps. Therefore it can be used to judge the quality of the plasmonic PSS. In our structures, the 170nm-diameter PSS reaches the side-band suppression S_{dB} =34dB at λ=568nm, and S_{dB} =31dB at λ=520nm, and the 260nm-diameter PSS reaches the side-band suppression S_{dB} =28dB at λ=568nm, and S_{dB} =26dB at λ=520nm (data shown in Table **I**), which can be compared with that of non-plasmonic grating coupler [S9, S10]. From Table **I**, it is interesting to see that PSS with smaller diameter has better side-band suppression than a larger one. It owes to better confinement of a smaller nanowire, which makes the manipulation of the grating more efficient. Thereafter the side-band suppression can be improved by changing the size of the nanowire.

In our case, the desired output light beams are designed out of the nanowire, and hence the outcoupling efficiency of each released light frequency is defined as

$$\eta(\lambda) = \frac{P(\lambda)}{P_0(\lambda)}, \quad (2)$$

where $P(\lambda)$ is the light power out of the grating, $P_0(\lambda)$ is the incident surface wave power propagating along the nanowire. Thus the value can be evaluated by the data in Fig. 3c, d and Fig. S5d,e. The outcoupling efficiency of 568nm light at “out-1” reaches about 47% in the 170nm-diameter PSS, while dramatically increases to 74% in the 260nm-diameter PSS. Similarly, the outcoupling efficiency of 520nm light at “out-2”

is about 6% in the 170nm-diameter PSS, while reaches to 17% in the 260nm-diameter PSS. From the data we can have two conclusions. Firstly, the outcoupling efficiency of the 260nm-diameter PSS is much larger than that of the 170nm-diameter. It is resulted from the effect of the size of nanowire on the SPs loss. Usually small structure has better confinement but with large loss. Secondly, the outcoupling efficiency dramatically attenuates from "out-1" to "out-2" due to the intrinsic loss of SPs.

4. Discrepancy between experiments and simulations

It can be seen from Fig. 3, 4 and Fig. S3, S4 although the experimental data agree with calculated ones, there are still discrepancies between experiments and simulations. The discrepancy, on one hand is due to the fact that the chemically-synthesized nanowire usually cannot generate nanowires with perfectly rounded cross-sectional shapes. Recently it has been studied that the cross-sectional shape of the nanowires will affect SPs propagation behavior [S11]; on the other hand, is resulted from the defects on the Ag nanowires (Fig. S9), which couldn't be taken account of in the calculations. Besides, due to the limitation of fabrication, the scratches on Si wafer cannot be avoided when milling the grooves on Ag nanowire by using FIB. These scratches also introduce mismatch between the experimental and calculated results.

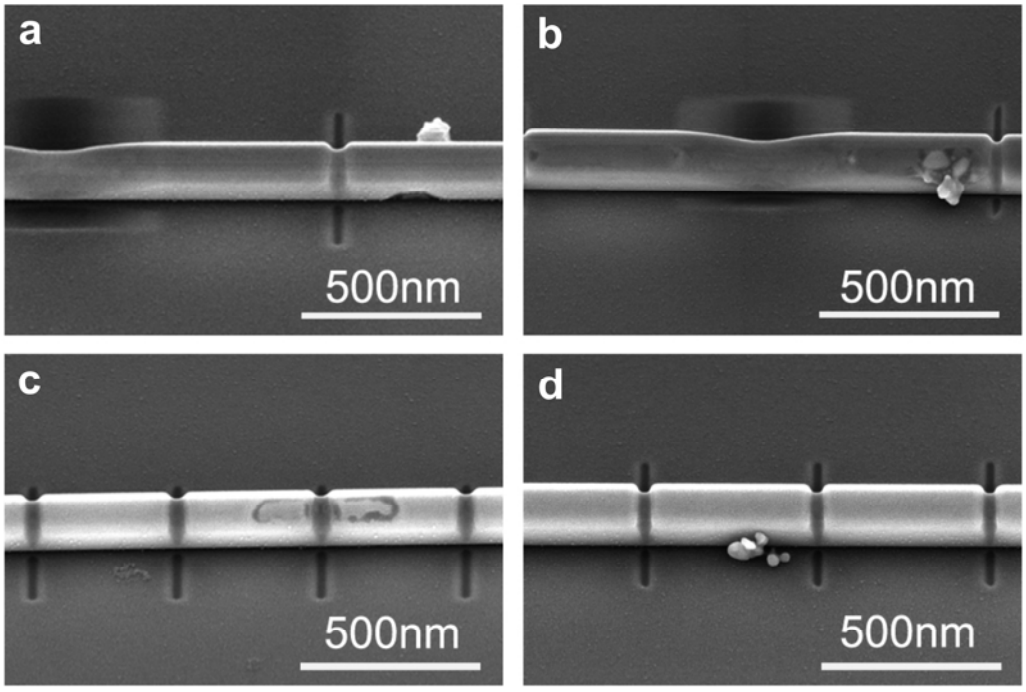

Supplementary Figure S9 | SEM images of Ag nanowires with defects.

5. Propagation performances of the plasmonic PSS and SOI nanowire at visible regime

Silicon-on-insulator (SOI) has received much attention and gain great achievement in the recent few years as it offers the possibility of integrating optical devices into electronic circuits by using the existing Si miscorelectrics fabrication technology. Currently, SOI waveguide based devices which operate at infrared wavelength of 1.3μm have already been integrated on submicro-size chip. Next we investigate the performances of the plasmonic PSS and SOI nanowire at visible regime by comparing the propagation length and mode confinement. Considering the top-down fabrication technology, the SOI nanowire may be easy to be fabricated to have a rectangle cross section. In the comparison, the Ag nanowire has a 170nm diameter and 5nm SiO_2 coating layer, which is exactly same as our experimental situation. In the SOI nanowire structure, a 50nm-thick SiO_2 spacer layer is positioned between the Si nanowire and Si substrate. The Si nanowire atop the SiO_2 has a square cross-sectional shape, whose side length equals the diameter of Ag nanowire. We calculate the propagation length and mode profile by using FDTD method (Lumerical 8.0.1) with a Gaussian source at 647nm operating wavelength. As shown in Fig. S10a, even within a 3μm distance the transportation energy in SOI nanowire is lower than 0.2 comparing with the input power. Hence the SOI nanowire fails to propagation the light at 647nm wavelength. The electric energy is confined around the Ag nanowire surface (Fig. S10b), while distributed in the whole Si nanowire area (Fig. S10d). These differences reveal the advantages of on-chip surface plasmonic devices at visible regime.

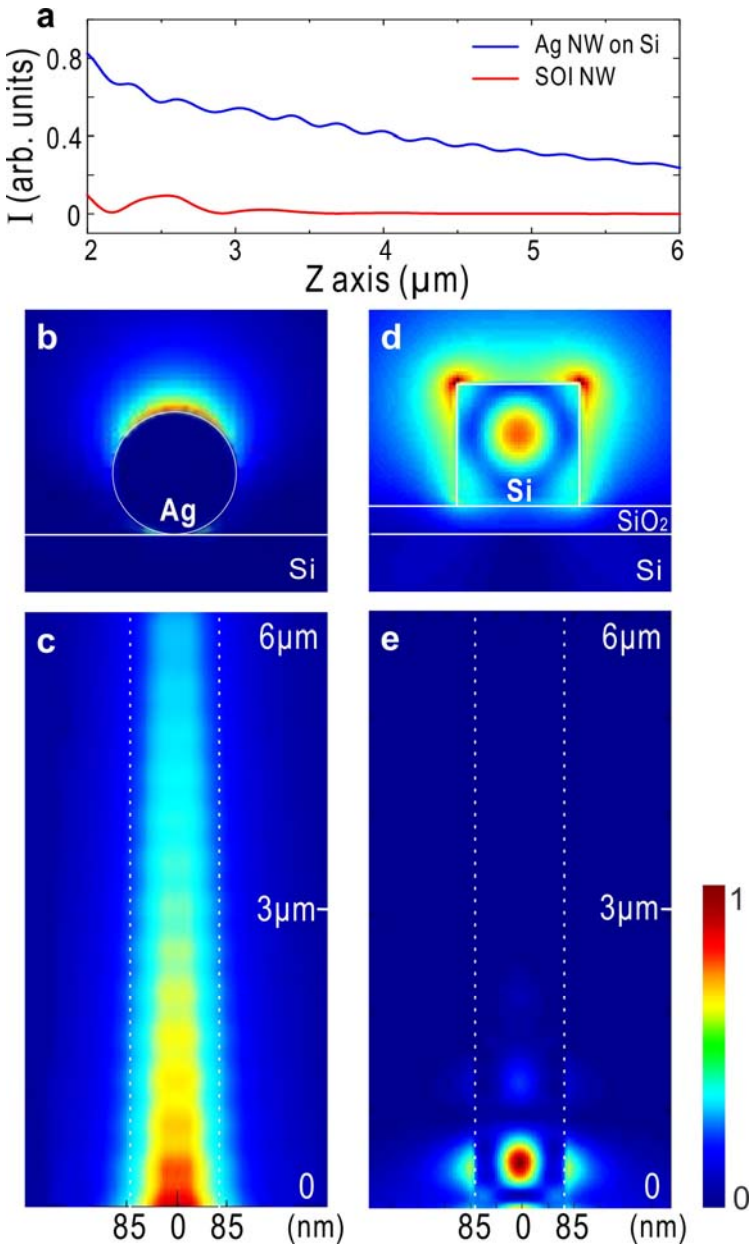

Supplementary Figure S10 | Propagation performance of the plasmonic PSS and SOI nanowire at visible regime. a. Normalized intensity **($|E|^2$)** collected from the output distal end of Ag nanowire (blue line) and SOI nanowire (red line) with different lengths. Mode profiles of **b.** Ag nanowire, **d.** SOI nanowire. Normalized intensity **($|E|^2$)** detected above a 6μm length **c.** Ag nanowire, **e.** Si nanowire. The observation plane of Ag nanowire is located at 10nm from the wire top, while the observation plane of Si nanowire is located at the center of the wire. In the SOI nanowire structure, the thickness of the spacer layer (SiO_2) between the Si nanowire and Si substrate is set as 50nm. Both the diameter of Ag nanowire and side width of Si nanowire are 170nm.

Reference:

S1. Sun, Y. G., et al. Polyol Synthesis of Uniform Silver Nanowires: A Plausible Growth Mechanism and the Supporting Evidence. *Nano. Lett.* **3**, 955 (2003).

S2. Sanders, A. W. et al. Observation of plasmon propagation, redirection, and fan-out in silver nanowires. *Nano Lett.* **6**, 1822–1826 (2006).

S3. Li, Z. et al. Effect of a proximal substrate on plasmon propagation in silver nanowires. *Phys. Rev. B.* **82**, 241402 (2010).

S4. Zhang, S. & Xu, H. Optimizing substrate-mediated plasmon coupling toward high-performance plasmonic nanowire waveguides. *ACS NANO* **6**, 8128-8135 (2012).

S5. Zou, C. L. et al. Plasmon modes of silver nanowire on a silica substrate. *Appl. Phys. Letts*. **97**, 183102 (2010).

S6. Oulton, R. F., Sorger, V. J., Genov, D. A., Pile, D. F. P., Zhang, X. A hybrid plasmonic waveguide for subwavelength confinement and long-range propagation. *Nature Photon.* **2**, 496-500 (2008).

S7. Handapangoda, D., Premaratne, M, Rukhlenko, I. D., Jagadish, C. Optimal design of composite nanowires for extended reach of surface plasmon-polaritons. *OPTICS EXPRESS* **19**, 16058-16074 (2011).

S8. Moharam, M. G., Grann, E. B., Pommet, D. A. Formulation for stable and efficient implementation of the rigorous coupled-wave analysis of binary gratings. *J. Opt. Soc. Am. A* **12**, 1068-1076 (1995).

S9. Nguyen, H. G et al. All optical up-coversion of WLAN signal in 60 GHz range with side-band suppression. *IEEE Radio and Wireless Symposium*, 590-593 (2009).

S10. Frankel, M. Y. & Esman, R. D. Optical single-sideband suppressed-carrier modulator for wide-band singnal processing. *J. Lightwave Technol*. **16**, 859-863 (1998).

S11. Wei, H. et al. Highly tunable propagating surface plasmons on supported silver nanowires. *PNAS*. **110**, 4494-4499 (2013).